

# *Suzaku* and *XMM-Newton* observations of a newly-discovered early-stage cluster merger 1E2216.0-0401 and 1E2215.7-0404

H. Akamatsu<sup>1</sup>, L. Gu<sup>1</sup>, T. W. Shimwell<sup>2</sup>, F. Mernier<sup>1,2</sup>, J. Mao<sup>1,2</sup>, I. Urdampilleta<sup>1,2</sup>,  
J. de Plaa<sup>1</sup>, H.J.A. Röttgering<sup>2</sup>, and J. S. Kaastra<sup>1,2</sup>

<sup>1</sup> SRON Netherlands Institute for Space Research, Sorbonnelaan 2, 3584 CA Utrecht, The Netherlands e-mail: h.akamatsu@sron.nl

<sup>2</sup> Leiden Observatory, Leiden University, PO Box 9513, 2300 RA Leiden, The Netherlands

## ABSTRACT

We present the results of *Suzaku* and *XMM-Newton* X-ray observations of the cluster pair 1E2216.0-0401 and 1E2215.7-0404. We discover an X-ray bridge between the clusters. *Suzaku* and *XMM-Newton* observations revealed that each cluster hosts gas with moderate temperature of  $kT_{0401} = 4.8 \pm 0.1$  keV and  $kT_{0404} = 5.8 \pm 0.2$  keV, respectively. On the other hand, the bridge region shows a remarkably high temperature ( $kT = 6.6 \pm 0.5$  keV). Furthermore, at the position of the bridge, we detected an enhancement in the wavelet-decomposed soft-band (0.5–4.0 keV) *XMM-Newton* image at 3 sigma significance, this is most likely due to a compression of the intracluster medium (ICM) as a consequence of the merging activity. This X-ray intensity and temperature enhancement are not consistent with those expected from a late phase, but are in agreement with the predictions by numerical simulations of an early phase merger. From the temperature jump at the location of the bridge, the Mach number is estimated to be  $M = 1.4 \pm 0.1$ , which corresponds to a shock propagation velocity of about 1570 km/s. From the shock properties, we estimate that core-passage will occur in 0.3–0.6 Gyr and that the age of the shock structure is 50–100 Myr. Based on the measured properties of the ICM at the bridge and estimation of timescales, we find indications for non-equilibrium ionization. We also discover possible diffuse radio emission located between the merging clusters. Combining the radio, X-ray, and optical image data, we speculate that the detected radio sources are most likely related to the merger event. Thus, 1E2216.0-0401 and 1E2215.7-0404 is a new example of an early phase cluster merger with remarkable characteristics.

**Key words.** galaxies: clusters: individual (1E2216.0-0401, 1E2215.7-0404), X-rays: galaxies: clusters

## 1. Introduction

According to the framework of hierarchical structure formation, galaxy clusters are the largest gravitationally bound objects in the Universe. Galaxy clusters are expected to grow via merging processes i.e. from collisions with smaller sub-haloes such as sub-clusters and groups of galaxies. Such cluster merging processes release up to  $\sim 10^{64}$  erg of kinetic energy into several channels such as heating due to merger induced shocks, turbulence and the amplification of the intergalactic magnetic field, etc. (Markevitch & Vikhlinin 2007). These non-thermal phenomena might (re-)accelerate (pre-accelerated) particles up to relativistic energies, producing synchrotron radio emission (for a review, see e.g. Feretti et al. 2012). The combination of X-ray and radio observations, therefore, has the strong advantage for understanding the cluster merging process and related phenomena. Knowledge of the cluster energy partition among different components is crucial information not only to understand its role in cluster evolution (e.g. Voit 2005) but also to construct cosmological probe (e.g. Allen et al. 2011).

Previously a handful of merging clusters were investigated in the X-ray band (e.g., Markevitch et al. 1999, 2002; Finoguenov et al. 2010; Russell et al. 2010, 2012; Macario et al. 2011; Ogrea & Brügggen 2013; Bourdin et al. 2013; Akamatsu & Kawahara 2013) and also see Markevitch (2010). However, most of these observed mergers are in a late phase (after core-crossing), because the early phase (before core-crossing) is relatively short-lived (e.g., Ricker & Sarazin

2001). Until now, there are 4 representative examples<sup>1</sup> of early phase cluster mergers: A399&A401 (Fujita et al. 1996, 2008), A1750 (Belsole et al. 2004; Bulbul et al. 2016), Cygnus A (Markevitch et al. 1999; Sarazin et al. 2013) and CIZA J1358.9-4750 (Kato et al. 2015). Although Kato et al. (2015) reported a signature of a merger shock in X-ray data, the other three early phase cluster mergers do not show any clear shock structure. Furthermore, no concrete evidence of the connection between radio emission and such shocks has been reported so far. Consequently, the physics of early phase cluster mergers remains poorly understood.

In this paper, we report a new example of an early phase cluster merger based on the results of *Suzaku* and *XMM-Newton* observations of 1E2216.0-0401 (RA = 22h18m40.5s, Dec = -03d46m48s:  $z=0.09$ : Cruddace et al. 2002) and 1E2215.7-0404 (RA = 22h18m17.1s, Dec = -03d50m03s:  $z=0.09$ : Gioia & Luppino 1994). We refer to these clusters as 0401 and 0404, respectively. Both clusters are separated by a projected distance of 640 kpc ( $\sim 7.2$  arcmin). We assume the cosmological parameters  $H_0 = 70$  km s<sup>-1</sup> Mpc<sup>-1</sup>,  $\Omega_M = 0.27$  and  $\Omega_\Lambda = 0.73$ . At a redshift of  $z=0.09$ , 1' corresponds to 91.8 kpc. As our fiducial reference for the solar photospheric abundances denoted by  $Z_\odot$ , we adopt Lodders et al. (2009). A Galactic absorption column of  $N_H = 7.3 \times 10^{20}$  cm<sup>-2</sup> (Willingale et al. 2013) was included in all fits. Unless otherwise stated, all our spectral analyses are done by

<sup>1</sup> We do not include A222&223 because of their large line-of-sight distance difference  $\sim 15$ –18 Mpc (Werner et al. 2008; Dietrich et al. 2012).

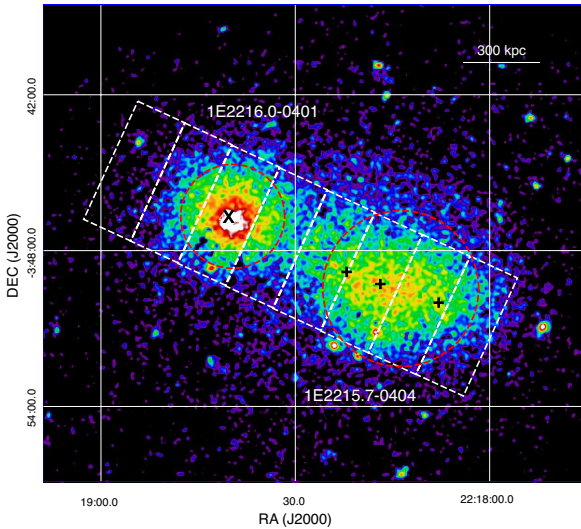


**Fig. 1.** Background-subtracted *XMM-Newton* image of 1E2216.0-0401 and 1E2215.7-0404 in the 0.8–8.0 keV band. The magenta circles and white boxes ( $2' \times 5'$ ) show the regions that we discuss in this letter. The  $\times$  and  $+$  indicate the dominant galaxy(ies) of each cluster.

using the Cash statistic (Cash 1979) and the errors correspond to 68% confidence for each parameter.

## 2. Observations and data reduction

*Suzaku* (Mitsuda et al. 2007) performed two observations covering both clusters (Fig. 1). The X-ray imaging sensor (XIS: Koyama et al. 2007) on board *Suzaku* consists of three front-side illuminated (FI) CCD chips (XIS0 and XIS3) and one back-side illuminated (BI) chip (XIS1). All observations were performed with either the normal  $5 \times 5$  or  $3 \times 3$  clocking mode. Data reduction was performed with HEASoft version 6.15 and CALDB version 20140624. We started with the standard data screening provided by the *Suzaku* team and applied an event screening with geomagnetic cosmic-ray cut-off rigidity ( $COR2$ )  $> 6$  GV to suppress the detector background. An additional screening was applied for the XIS1 detector to minimize the detector background. We followed the processes described in the *Suzaku* XIS official document<sup>2</sup>. The positions of the calibration sources and the failing area in XIS0 were excluded<sup>3</sup>. The resultant clean exposure times are 25 and 11 ks, respectively. The observational information is shown in Tab. 1.

*XMM-Newton* was used to observe 1E2216.0-0401 on 2011 June 13 for a short exposure of 15.9 ks. The SAS v13.5 and the built-in extended source analysis software (ESAS) were utilized to process and calibrate the data obtained with the *XMM-Newton* European Photon Imaging Camera (EPIC). Following a standard procedure, the MOS raw data were created by `emchain`, and the lightcurves were extracted and screened for time variable background component by the `mos-filter` task. The final net clean exposures are 10.5 ks, 13.5 ks, and 6.7 ks for the MOS1, MOS2, and pn data, respectively. The observational information is shown in Tab. 1.

<sup>2</sup> [http://www.astro.isas.jaxa.jp/suzaku/analysis/xis/xis1\\_ci\\_6\\_nxb/](http://www.astro.isas.jaxa.jp/suzaku/analysis/xis/xis1_ci_6_nxb/)

<sup>3</sup> <http://www.astro.isas.jaxa.jp/suzaku/doc/suzakumemo/suzakumemo-2010-01.pdf>.

**Table 1.** Observational log

	ID	R.A., DEC (J2000)	Observation Starting date	Exp (ks)
<i>Suzaku</i>	807085010	334.65, -3.76	2012-05-16	24.9
	807084010	334.58, -3.85	2012-11-29	11.2
<i>XMM</i> <sup>a</sup>	677180101	334.57, -3.83	2011-06-13	10.5, 13.5, 6.7

<sup>a</sup>: Exposure times are for EPIC MOS1, 2 and pn

**Table 2.** *Suzaku* best-fit parameters for each cluster and for the bridge region

	$kT$ (keV)	$Z$ ( $Z_{\odot}$ )	Norm ( $10^{70}/\text{m}^3/\square'$ )	C-stat/d.o.f.
0401	$4.75 \pm 0.10$	$0.33 \pm 0.04$	$31.3 \pm 0.5$	1130 / 1085
0404	$5.68 \pm 0.18$	$0.33 \pm 0.04$	$18.1 \pm 0.8$	1230 / 1229
Bridge	$6.63 \pm 0.48$	0.3 (fix)	$14.5 \pm 1.3$	342 / 311

## 3. Spectral analysis and result

### 3.1. Spectral analysis approach

For the spectral analysis of *Suzaku* data, we used the SPEX (Kaastra et al. 1996) software version 3.01.00. Each spectrum was binned based on the “optimal binning” method (Kaastra & Bleeker 2016). The best-fit parameters were obtained by minimizing the C-stat. In all the spectral analysis results presented here, the detector background (Non X-ray Background: NXB) was estimated from the night Earth data base using `xisnxbgen` (Tawa et al. 2008) and subtracted from the observed spectra. Other background components such as Galactic emission and unresolved X-ray sources (Cosmic X-ray background: CXB) are modeled during the fitting procedure. For the spectral fitting, we used the energy ranges of 0.8–8.0 keV for both detectors. To estimate exactly the responses of the X-ray telescope and XIS, we employed the Monte Carlo simulator `xissimarfgen` (Ishisaki et al. 2007). As an input image, we employed a flat field emission model ( $r=20'$ ). For the Galactic background components, we used two thermal (the `cie` model in SPEX) components: one is unabsorbed and another is absorbed. In both components, we fixed the abundance and the redshift to unity and zero, respectively. Furthermore, we fixed the temperature of each component to 0.08 keV and 0.3 keV, respectively. For the fitting, we kept the normalization of thermal components free. For the CXB component, we refer to Kushino et al. (2002). In total, we used the spectral model: `cie + abs * (cie + Powerlaw + cieICM)`. Because of the energy range which was used for the fitting, our results are insensitive to the Galactic background components.

The *XMM-Newton* source spectra, NXB, and response files were prepared by the `mos-spectra` task. The CXB and two Galactic foreground components were calculated in the same way for the *Suzaku* analysis. To complement the limited angular resolution of the *Suzaku* XRT (HPD $\sim 2'$ : Serlemitsos et al. 2007), we used *XMM-Newton* images to identify and evaluate the fluxes of point sources, which were detected by the `cheese` task above a flux threshold of  $5 \times 10^{-14}$  ergs  $\text{cm}^{-2}$   $\text{s}^{-1}$ . These point sources were excluded in all the subsequent spectral analysis.

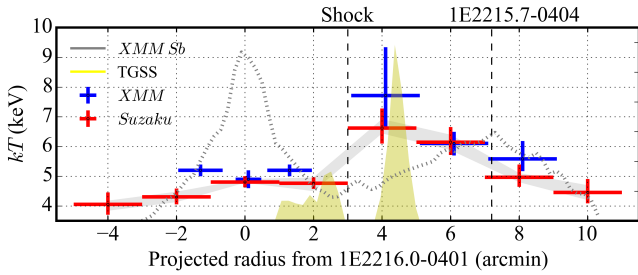


**Fig. 2.** Radial temperature profile from 1E2216.0-0401. Red and blue crosses show *Suzaku* and *XMM-Newton* results, respectively. The dashed line indicates the *XMM-Newton* 0.5–7.0 keV surface brightness profile. The gray range represent the uncertainties of *Suzaku* temperature estimation due to the combined 3% variation of the NXB level and the 30% fluctuation in the CXB. The yellow region shows GMRT 154 MHz radio emission. The bins of *XMM-Newton* are slightly offset (0.1') for clarity.

### 3.2. Results

For the first step, to understand the global properties of each cluster, we extracted spectra from circular regions centred on 0401 and 0404 with  $r=2'$  and  $r=3'$ , respectively. The best-fit values are listed in Tab. 2. Both clusters show similar values for the temperature ( $kT_{0401} = 4.8 \pm 0.1$  keV,  $kT_{0404} = 5.7 \pm 0.2$  keV) and the abundance ( $Z_{0401} = 0.33 \pm 0.04 Z_{\odot}$ ,  $Z_{0404} = 0.33 \pm 0.04 Z_{\odot}$ ). The redshifts derived for the clusters are  $z_{0401} = 0.093 \pm 0.001$  and  $z_{0404} = 0.091 \pm 0.001$ . The velocity difference derived from the redshifts  $\Delta v \sim 600$  km/s is smaller than the sound speed (galaxy velocity dispersion) of each cluster ( $c_s \sim 1100$  km/s). Thus the two clusters are at a similar line-of-sight distance.

In order to investigate the temperature structure in the direction of the merging axis (0401 to 0404), we extracted spectra in 8 boxes ( $2' \times 5'$ : 182 kpc  $\times$  460 kpc), as shown in Fig. 1. We followed the same procedure described above but fixed the abundance to  $0.3Z_{\odot}$  (e.g., Fujita et al. 2008).<sup>4</sup> To investigate the influence of uncertainties in the background components in the *Suzaku* data, we considered 30% and 3% fluctuations of the intensity of the CXB and the NXB components (Tawa et al. 2008). Because we did not use the low-energy band, the effect of the Galactic background is limited. Therefore, we did not consider this systematic error.

The resultant temperature profile is shown in Fig. 2, where red and blue crosses represent the best fit value of *Suzaku* and *XMM-Newton*, respectively. In general, the results of *Suzaku* and *XMM-Newton* are consistent with each other within the statistical uncertainties (68 % significance). The basic feature of the profile is insensitive to the systematic error of the background components (gray shallow region). Between both clusters ( $r=3.0' - 5.0'$ ), the ICM shows a clear enhancement from  $kT_{r=1'-3'} = 4.7$  keV in the cluster centres to  $kT_{Bridge, Suzaku} = 6.6$  keV in the region between the clusters. We also found an enhancement of the surface brightness in the 0.5–4.0 keV *XMM-Newton* image (Fig. 2 and 3).

To detect enhanced ICM structure in the connecting region, we apply a wavelet decomposition based on the à Trous transform (e.g., Gu et al. 2009) on the vignetting-corrected *XMM-Newton* image. By masking out coefficients within  $3\sigma$  fluctuations of the background region, and reconstructing the features

<sup>4</sup> Considering the difference between the two solar abundance tables, the Fe abundance in this latter is 1.5 times higher than that of Fujita et al. (2008).

with scales above  $\sim 100$  kpc, we obtained a significant coefficient map as shown in Fig. 3 right. The observed features, such as the shock heated and compressed region between both clusters, are in good agreement with predictions by numerical simulations (Takizawa 1999; Akahori & Yoshikawa 2010).

The structure located between the clusters and centered on the high temperature region, suggests the presence of a pressure discontinuity, that is, the presence of a shock front.

## 4. Discussion

The observation of a clear shock structure in an early phase cluster merger is not so common so far. In order to understand the nature of early phase cluster mergers, additional examples are of importance.

The observational features revealed by *Suzaku* and *XMM-Newton* can not be explained by the late phase of a merger. Furthermore, based on available optical information, we found the presence of some peculiar galaxies in 0401 and 0404. The positions of these galaxies are roughly consistent with the X-ray peak of each cluster ( $\times$  and  $+$  in Fig. 1). This indicates that the ICM of each cluster has not been perturbed for a long time by the merger. Most likely the clusters are before core-crossing (early merger phase) but when they are close enough to interact and form a shock front.

The *Suzaku* and *XMM-Newton* temperature profiles show a clear jump at the bridge region, indicating the presence of a shock front. Here we evaluate the properties of this shock structure based only on the *Suzaku* measurements because of they have a lower particle background and longer observation time. The Mach number  $\mathcal{M}$  can be estimated by applying the Rankine-Hugoniot jump condition (Landau & Lifshitz 1959),  $\frac{T_2}{T_1} = \frac{5\mathcal{M}^4 + 14\mathcal{M}^2 - 3}{16\mathcal{M}^2}$  assuming the ratio of specific heats as  $\gamma = 5/3$  and 1,2 denote pre-shock and post-shock, respectively. Substituting the pre- and post-shock temperature  $T_1 = 4.7 \pm 0.2$  keV and  $T_2 = 6.6 \pm 0.5$  keV into the above equation gives a Mach number  $\mathcal{M}_{Suzaku} = 1.4 \pm 0.1$ . Following equation (2) in Markevitch et al. (1999), the shock compression  $C$  can be estimated from the measured temperature ratio. Substituting the pre- and post-shock temperature ratio into the equation gives a shock compression  $C \sim 1.56$ . The heating due to adiabatic compression is expected to be about  $T_2 = T_1 \cdot C^{\gamma-1} \sim 6.3$  keV, in good agreement with the post-shock temperature. Thus, the dominant part of the heating is carried out by adiabatic compression. The estimated low Mach number and heating mechanism are consistent with the properties of a shock structure that cosmological simulations predict to occur in an early-phase cluster merger (e.g., Miniati et al. 2000; Ricker & Sarazin 2001; Ryu et al. 2003).

Combining the sound speed at the pre-shock region ( $c_s \sim 1150$  km  $s^{-1}$ ) with the Mach number, the shock propagation velocity is estimated to be about 1570 km/s. With the assumption that the clusters move with the same velocity, we estimate that “the core passing” will occur in 0.3–0.6 Gyr. Under the same assumption, the age of the shock is also estimated to be 50–100 Myr.

Due to the low density environment at cluster outskirts, it is commonly believed that non-equilibrium ionization and electron-ion temperature structure remain just after the shock because it has not had enough time to equilibrate (Takizawa & Mineshige 1998; Rudd & Nagai 2009; Akahori & Yoshikawa 2010). The equilibration time scales

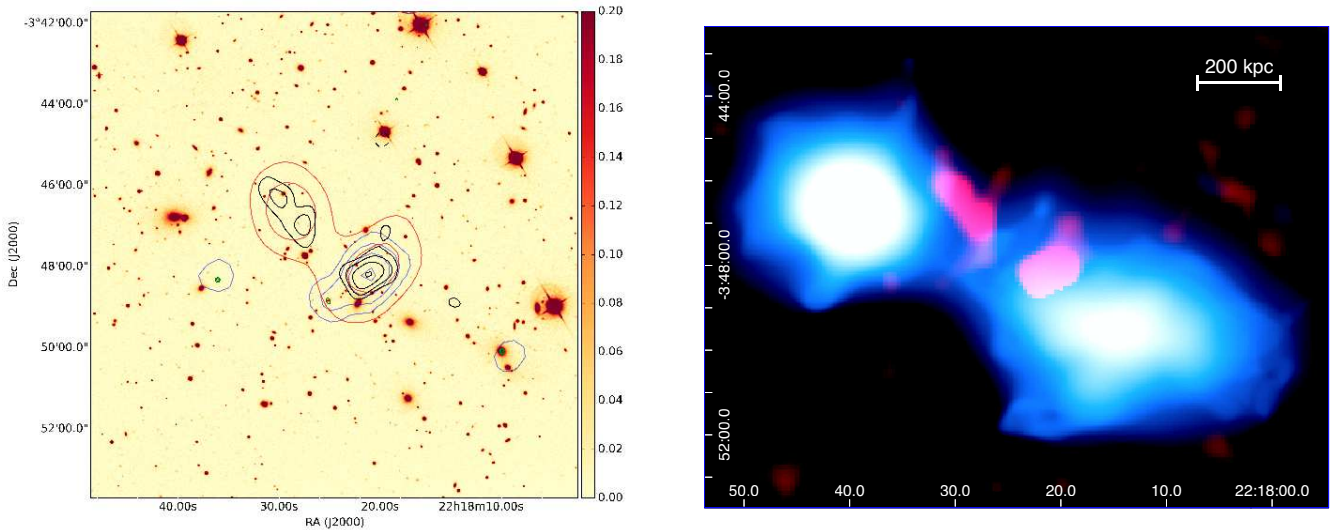


**Fig. 3.** Left: the radio emission from VLSSr, TGSS, FIRST, and NVSS in red, black, green and blue respectively. The contours are at  $(1, 2, 4, \dots) \times 4 \times \sigma$  levels where  $\sigma$  is 90 mJy/beam, 6.0 mJy/beam, 0.24 mJy/beam and 0.6 mJy/beam for the VLSSr, TGSS, FIRST and NVSS respectively. The radio emission is overlaid on an SDSS r-band image of the region. Right: wavelet-decomposed 0.5–4.0 keV *XMM-Newton* image in blue. We show sources with  $> 3\sigma$  significance and scales above  $\sim 100$  kpc. The filamentary structure between two halos is visible in the image. The red shows the 154MHz radio intensity from the TGSS alternative data release (Intema et al. 2016). Furthermore, there is a structure in the X-ray image at the bridge, which might be the shock compressed ICM region.

of non-equilibrium ionization  $t_{\text{CIE}}$  and electron-ion two temperature structure  $t_{\text{ie}}$  (Spitzer 1956; Masai 1984; Takizawa 1998) can be described as  $t_{\text{CIE}} \sim 3 \times 10^9 \left(\frac{n_e}{10^{-4} \text{ cm}^{-3}}\right)^{-1} \text{ yr}$ ,  $t_{\text{ie}} \sim 2 \times 10^9 \left(\frac{n_e}{10^{-4} \text{ cm}^{-3}}\right)^{-1} \left(\frac{T}{10^8 \text{ K}}\right)^{\frac{3}{2}} \text{ yr}$ , respectively. Here, we estimate the electron density of the bridge region from the *cie* normalization ( $norm = n_e n_X V$ ). Assuming a 2 Mpc line of sight depth and the normalization value of the unit area (Tab.2), the electron density at the shock heated region is estimated to be  $n_e = 6.0 \times 10^{-4} (l/2\text{Mpc})^{-0.5} \text{ cm}^{-3}$ , where  $l$  is the line-of-sight depth. We note that  $l$  is quite unconstrained, hence  $n_e$  is rather uncertain. Combining with the assumption of  $l = 2$  Mpc and the measured shock temperature, the equilibration timescales are estimated to be  $t_{\text{CIE}} \sim 0.5$  Gyr and  $t_{\text{ie}} \sim 0.2$  Gyr. These timescales are longer than the estimated age of the shock structure estimated from the shock propagation velocity, indicating a part of the shock heated region would not have reached equilibrium yet.

To investigate the possibility of a non-equilibrium ionization state, we evaluated the  $rt$  parameter in the *cie* model, which represents the ratio of ionization balance temperature to electron temperature. The resultant value ( $rt = 0.45_{-0.10}^{+0.38}$ ) suggests that the ICM at the shock region has not yet reached ionization equilibrium, which will lead to an underestimation of the post-shock temperature. Furthermore we note that *Suzaku*'s large PSF might lead to a similar effect due to the effects of smearing. Therefore, the estimated Mach number is a lower limit. We stress that it is a challenge to make a firm conclusion about non-equilibrium ionization states with the currently available X-ray data. Deep X-ray observations are strongly desired. Future high resolution X-ray spectrometers such as the *Athena* X-IFU instrument (Ravera et al. 2014) will enable us not only to investigate these non-equilibrium states but also detailed spectroscopic diagnostics (e.g., Kaastra et al. 2009).

Diffuse radio emission is observed to be associated with the ICM of approximately 100 galaxy clusters and is generally thought to be formed as a consequence of shocks and turbulence in massive clusters (see e.g. Feretti et al. 2012 and

Brunetti & Jones 2014 for recent reviews). To search for such diffuse radio emission from the ICM of this merging cluster system and to characterise it as a function of frequency and resolution we have used the following wide-area radio surveys: the 74 MHz VLA Low-Frequency Sky Survey (VLSSr; Lane et al. 2012), the 150 MHz TIFR GMRT Sky Survey alternative data release (TGSS; Intema et al. 2016), the 1.4 GHz NRAO/VLA Sky Survey (NVSS; Condon et al. 1998), and the 1.4 GHz Faint Radio Images of the Sky at Twenty-Centimeters (FIRST; Becker et al. 1995). We find that in the vicinity of 0401 and 0404 there are two main regions of diffuse radio emission which are approximately coincident with the X-ray observed bridge between the clusters, these are object A at 22:18:22 - 03:48:08 and object B at 22:18:29 - 03:46:42. From the radio survey images we estimate that for object A the 150 MHz integrated brightness is  $570 \pm 60$  mJy and the 74 MHz to 1.4 GHz spectral index is  $-1.2 \pm 0.1$ , whereas for object B the integrated 150 MHz brightness is  $350 \pm 50$  mJy and the 74 MHz to 150 MHz spectral index is  $-2.0 \pm 0.3$  (object B is not detected in the 1.4 GHz images). Steep spectral indices together with the lack of an obvious optical counterpart or compact radio core (see Fig.3 left) are properties that are expected for radio emission that is associated with or influenced by shocks and turbulence in the ICM. Furthermore, such a classification is supported by the clear merging nature of the system and the close proximity of the radio emission and the X-ray detected shock. However, before any definitive classification of this radio emission is made it is important that more sensitive and higher resolution radio observations are conducted to thoroughly assess the morphological, spectral and polarisation properties of the emission.

In this paper we showed that 1E2216.0-0401 and 1E2215.7-0404 are a new example of an early phase cluster merger with a clear signature of a merger induced shock front and possibility of diffuse radio emission which also may relate to the merging activity. Further investigation with high spatial and spectral resolution X-ray observatories (*XMM-Newton*, *Chandra* and also *Athena*), sensitive radio observations (GMRT, JVLA and LO-FAR), weak lensing mass maps, and sophisticated numerical

simulations will provide us with deeper insight of the cluster merger dynamics and the origin of the diffuse radio emission.

## Acknowledgments

The authors wish to thank the referee for constructive comments that improved the manuscript. The authors thank the *Suzaku* and *XMM-Newton* team members for their support on the projects. H.A acknowledges the support of NWO via a Veni grant. SRON is supported financially by NWO, the Netherlands Organization for Scientific Research.

## References

- Akahori, T. & Yoshikawa, K. 2010, PASJ, 62, 335  
 Akamatsu, H. & Kawahara, H. 2013, PASJ, 65, 16  
 Allen, S. W., Evrard, A. E., & Mantz, A. B. 2011, ARA&A, 49, 409  
 Becker, R. H., White, R. L., & Helfand, D. J. 1995, ApJ, 450, 559  
 Belsole, E., Pratt, G. W., Sauvageot, J.-L., & Bourdin, H. 2004, A&A, 415, 821  
 Bourdin, H., Mazzotta, P., Markevitch, M., Giacintucci, S., & Brunetti, G. 2013, ApJ, 764, 82  
 Brunetti, G. & Jones, T. W. 2014, International Journal of Modern Physics D, 23, 30007  
 Bulbul, E., Randall, S. W., Bayliss, M., et al. 2016, ApJ, 818, 131  
 Cash, W. 1979, ApJ, 228, 939  
 Condon, J. J., Cotton, W. D., Greisen, E. W., et al. 1998, AJ, 115, 1693  
 Cruddace, R., Voges, W., Böhringer, H., et al. 2002, ApJS, 140, 239  
 Dietrich, J. P., Werner, N., Clowe, D., et al. 2012, Nature, 487, 202  
 Feretti, L., Giovannini, G., Govoni, F., & Murgia, M. 2012, A&A Rev., 20, 54  
 Finoguenov, A., Sarazin, C. L., Nakazawa, K., Wik, D. R., & Clarke, T. E. 2010, ApJ, 715, 1143  
 Fujita, Y., Koyama, K., Tsuru, T., & Matsumoto, H. 1996, PASJ, 48, 191  
 Fujita, Y., Tawa, N., Hayashida, K., et al. 2008, PASJ, 60, 343  
 Gioia, I. M. & Luppino, G. A. 1994, ApJS, 94, 583  
 Gu, L., Xu, H., Gu, J., et al. 2009, ApJ, 700, 1161  
 Intema, H. T., Jagannathan, P., Mooley, K. P., & Frail, D. A. 2016, ArXiv e-prints  
 Ishisaki, Y., Maeda, Y., Fujimoto, R., et al. 2007, PASJ, 59, 113  
 Kaastra, J. S. & Bleeker, J. A. M. 2016, A&A, 587, A151  
 Kaastra, J. S., Bykov, A. M., & Werner, N. 2009, A&A, 503, 373  
 Kaastra, J. S., Mewe, R., & Nieuwenhuijzen, H. 1996, in UV and X-ray Spectroscopy of Astrophysical and Laboratory Plasmas, ed. K. Yamashita & T. Watanabe, 411–414  
 Kato, Y., Nakazawa, K., Gu, L., et al. 2015, PASJ, 67, 71  
 Koyama, K., Tsunemi, H., Dotani, T., et al. 2007, PASJ, 59, 23  
 Kushino, A., Ishisaki, Y., Morita, U., et al. 2002, PASJ, 54, 327  
 Landau, L. D. & Lifshitz, E. M. 1959, Fluid mechanics  
 Lane, W. M., Cotton, W. D., Helmboldt, J. F., & Kassim, N. E. 2012, Radio Science, 47, RS0K04  
 Lodders, K., Palme, H., & Gail, H.-P. 2009, Landolt Börnstein  
 Macario, G., Markevitch, M., Giacintucci, S., et al. 2011, ApJ, 728, 82  
 Markevitch, M. 2010, ArXiv e-prints  
 Markevitch, M., Gonzalez, A. H., David, L., et al. 2002, ApJ, 567, L27  
 Markevitch, M., Sarazin, C. L., & Vikhlinin, A. 1999, ApJ, 521, 526  
 Markevitch, M. & Vikhlinin, A. 2007, Phys. Rep., 443, 1  
 Masai, K. 1984, Ap&SS, 98, 367  
 Miniati, F., Ryu, D., Kang, H., et al. 2000, ApJ, 542, 608  
 Mitsuda, K., Bautz, M., Inoue, H., et al. 2007, PASJ, 59, 1  
 Ogrea, G. A. & Brüggem, M. 2013, MNRAS, 433, 1701  
 Ravera, L., Barret, D., den Herder, J. W., et al. 2014, in Proc. SPIE, Vol. 9144, Space Telescopes and Instrumentation 2014: Ultraviolet to Gamma Ray, 91442L  
 Ricker, P. M. & Sarazin, C. L. 2001, ApJ, 561, 621  
 Rudd, D. H. & Nagai, D. 2009, ApJ, 701, L16  
 Russell, H. R., McNamara, B. R., Sanders, J. S., et al. 2012, MNRAS, 423, 236  
 Russell, H. R., Sanders, J. S., Fabian, A. C., et al. 2010, MNRAS, 406, 1721  
 Ryu, D., Kang, H., Hallman, E., & Jones, T. W. 2003, ApJ, 593, 599  
 Sarazin, C. L., Finoguenov, A., & Wik, D. R. 2013, Astronomische Nachrichten, 334, 346  
 Serlemitsos, P. J., Soong, Y., Chan, K.-W., et al. 2007, PASJ, 59, 9  
 Spitzer, L. 1956, Physics of Fully Ionized Gases  
 Takizawa, M. 1998, ApJ, 509, 579  
 Takizawa, M. 1999, ApJ, 520, 514  
 Takizawa, M. & Mineshige, S. 1998, ApJ, 499, 82  
 Tawa, N., Hayashida, K., Nagai, M., et al. 2008, PASJ, 60, 11  
 Voit, G. M. 2005, Reviews of Modern Physics, 77, 207  
 Werner, N., Finoguenov, A., Kaastra, J. S., et al. 2008, A&A, 482, L29  
 Willingale, R., Starling, R. L. C., Beardmore, A. P., Tanvir, N. R., & O'Brien, P. T. 2013, MNRAS, 431, 394